

**Size and transparency influence diel vertical
migration patterns in copepods.**

Alex Barth^{*1}, Rod Johnson² and Joshua Stone¹

1. University of South Carolina, Biological Sciences, 700 Sumter St
401, Columbia, SC 29208
2. Bermuda Institute of Ocean Sciences, Bermuda GE 01, UK

² **0.1 Scientific Significance Statement**

³ **0.1.1 Study Novelty**

⁴ Diel Vertical Migration is a widespread phenomenon across marine and fresh-
⁵ water systems. The predator evasion hypothesis suggests that DVM occurs as
⁶ zooplankton attempt to escape visual predators. Yet, DVM itself is a costly
⁷ and risky behavior. Thus, DVM should only occur when visual risk is high.
⁸ Several studies have shown that copepod size influences the magnitude of DVM.
⁹ However, an individual's visual risk may include traits beyond simply size. In
¹⁰ this study, we utilize an in-situ imaging tool to reveal how copepod morpholog-
¹¹ ical traits influence DVM. Our findings show that both size and transparency
¹² influence DVM. We support this finding through rigorous statistical analyses
¹³ and state-of-the-art technology. This finding provides support for leading DVM
¹⁴ hypotheses and highlights that DVM is a complex behavior driven by multiple
¹⁵ copepod traits. Furthermore, this study represents a novel application of in-situ
¹⁶ imaging technology to address major hypotheses in biological oceanography.

¹⁷ **0.1.2 Applicability to L&O**

¹⁸ This study addresses diel vertical migration, an active, major research topic in
¹⁹ biological oceanography. Many studies published in L&O contribute to advanc-
²⁰ ing knowledge on DVM. In this paper, we provide strong evidence for both size
²¹ and transparency influencing DVM behavior. Additionally, we accomplished
²² this study using emerging technology and statistical analyses. This work builds
²³ on research published in L&O and will be broadly applicable to plankton ecol-

²⁴ ogists, biological oceanographers.

²⁵ AB and JS developed the study hypotheses. JS coordinated deployment and
²⁶ data management of the UVP. RJ facilitated data collection on cruises. AB
²⁷ led the analysis and preparation of the manuscript and figures. JS and RJ
²⁸ contributed to the manuscript draft. All authors approved the final submission.

²⁹ 1 Abstract

³⁰ Diel vertical migration (DVM) is a widespread phenomenon in aquatic envi-
³¹ ronments. The primary hypothesis explaining DVM is the predation-avoidance
³² hypothesis, which suggests that zooplankton migrate to deeper waters to avoid
³³ detection during daylight. Copepods are the predominant mesozooplankton
³⁴ undergoing these migrations, however they display massive morphological vari-
³⁵ ation. Visual risk also depends on a copepod's morphology. In this study, we
³⁶ investigate hypotheses related to morphology and DVM: (H1) as size increases
³⁷ visual risk, increases in body size will increase DVM magnitude and (H2) if cope-
³⁸ pod transparency can reduce visual risk, increases in transparency will reduce
³⁹ DVM magnitude. In-situ copepod images were collected across several cruises
⁴⁰ in the Sargasso Sea using an Underwater Vision Profiler 5. Copepod morphol-
⁴¹ ogy was characterized from these images and a dimension reduction approach.
⁴² While in-situ imaging offers challenges for quantifying mesozooplankton behav-
⁴³ ior, we introduce a robust method for quantifying DVM. The results show a clear
⁴⁴ relationship in which larger copepods have a larger DVM signal. Darker cope-

⁴⁵ pods also have a larger DVM signal, however only amongst the largest group
⁴⁶ of copepods and not smaller ones. These findings highlight the complexity of
⁴⁷ copepod morphology and DVM behavior.

⁴⁸ 2 Introduction

⁴⁹ Diel vertical migration (DVM) is a wide spread phenomena with large conse-
⁵⁰ quences in ocean ecosystems. DVM is the process of pelagic organisms verti-
⁵¹ cally moving in the water column on a daily basis, often travelling dozens to
⁵² hundreds of meters (Bianchi and Mislan 2016). This large-scale event occurs
⁵³ across many taxa, from plankton to fish (Brierley 2014). However, DVM is
⁵⁴ particularly notable in zooplankton communities, whose migrations contribute
⁵⁵ substantially to biogeochemical cycles (Steinberg and Landry 2017; Archibald et
⁵⁶ al. 2019; Siegel et al. 2023). Mesozooplankton communities, largely dominated
⁵⁷ by copepods (Turner 2004), will feed in surface layers of the ocean at night then
⁵⁸ migrate into deeper waters during daytime. Through this movement, copepods
⁵⁹ actively transport carbon to depth. Additionally, Kelly et al. (2019) described
⁶⁰ zooplankton DVM to be a major component of mesopelagic food webs. Thus to
⁶¹ understand pelagic food webs and nutrient cycles, it is critically important to
⁶² understand the drivers of DVM.

⁶³ DVM has long been studied in marine systems (Bandara et al. 2021). Predom-
⁶⁴ inantly, zooplankton DVM is the movement from deep waters at daytime to
⁶⁵ shallower waters at night (Hays 2003; Bianchi and Mislan 2016). However, re-

66 verse migration is also well documented (Ohman 1990). The adaptive benefits of
67 DVM have been extensively reviewed (Lampert 1989; Hays 2003; Cohen and For-
68 ward Jr. 2009; Ringelberg 2009; Williamson et al. 2011; Bandara et al. 2021).
69 Some studies have hypothesized that DVM provides a physiological advantage.
70 It has been suggested that moving to deeper waters may provide zooplankton
71 a reduction in UV-damage (Ewald 1912; Kessler et al. 2008), metabolic ben-
72 efits (McLaren 1963; Enright 1977), or demographic benefits (McLaren 1974).
73 However, the predator-avoidance hypothesis has received the most support to
74 explain ultimate causes of DVM (see review of current evidence by Bandara et
75 al. 2021). First described by Zaret and Suffern (1976), this hypothesis posits
76 zooplankton evacuate the sunlit surface to evade visual predators then ascend
77 at night to feed. However the massive migration undertaken by zooplankton
78 is energetically expensive (Maas et al. 2018; Robison et al. 2020). Therefore,
79 the predator-avoidance hypothesis makes a clear prediction that the trade-off of
80 expended energy is worth the predator avoidance benefit (Lampert 1989). This
81 trade-off has been further described in observations of the relationship between
82 zooplankton feeding and DVM patterns which led to the hunger-satiation hy-
83 pothesis (Atkinson et al. 1992; Pearre 2003). This hypothesis suggests that
84 vertical migrators will ascend to feed when hungry then retreat once full. Once
85 an individual has fully fed, remaining at the surface provides no benefit while
86 their visual risk may increase due to their full guts which may increase visibility.
87 Thus, the hunger-satiation hypothesis provides a detailed case of the predato-
88 avoidance hypothesis and suggests cases where copepods may forego DVM. Re-

89 gardless, both the hunger-satiation hypothesis and the predator-avoidance hy-
90 pothesis suggest DVM is primarily a result of top-down control. In modelling
91 studies with copepods, the predominant oceanic zooplankton, top-down con-
92 trol (Bandara et al. 2019) and trophic interactions (Pinti et al. 2019) have
93 successfully been used to replicate DVM patterns.

94 Predator-driven migration suggests that DVM can be a function of an individual
95 copepod's detection risk by a visual predator. However, this risk can depend on
96 a copepod's morphological features (Aksnes and Utne 1997). Notably a cope-
97 pod's size can increase visual detection. Several studies have documented that
98 copepod size influences DVM magnitude (Hays et al. 1994; Ohman and Ro-
99 magnan 2016; Aarflot et al. 2019). Presumably, a copepod's transparency will
100 also influence DVM. Hays et al. (1994) reported that pigmentation explained
101 variation in DVM frequency. However, few other studies have investigated this
102 at length. One barrier to studying a relationship between copepod morphology
103 and DVM is the difficulty of accurately recording traits. Several approaches
104 have been utilized to study DVM. High spatiotemporal resolution of DVM can
105 be achieved through acoustic (Liu et al. 2022), and even satellite-based mea-
106 surements (Behrenfeld et al. 2019). However these approaches do not yield
107 information about individuals, much less traits. Net collected specimens can al-
108 low for trait-related investigations of copepod DVM patterns (Hays et al. 1994;
109 Ohman and Romagnan 2016). However, it is much more challenging to measure
110 traits related to copepod transparency from net-collected specimens. Copepods
111 collected from deep net tows can be severely damaged and their gut contents

112 may not reflect natural conditions due to cod-end feeding or regurgitation. Fur-
113 thermore, typical preservation methods of net-specimens can result in the loss
114 of pigmentation through bleaching in ethanol or formalin or increases in opacity
115 as the copepod dies. Yet traits related to copepod's transparency are not well
116 captured in net-collected specimens which may evacuate gut contents or lose pig-
117 mentation following preservation in formalin or ethanol. In Hays et al. (1994)'s
118 investigation, the authors relied on previously published copepod carotenoid
119 values in their analyses rather than attempt to measure pigment values from
120 their preserved specimens.

121 However, these sampling challenges may be effectively circumvented with the
122 emerging use of in-situ imaging tools. By directly observing copepods, new
123 insights into their behavior and traits can be resolved (Ohman 2019). For ex-
124 ample, Whitmore and Ohman (2021) used an in-situ imaging device to describe
125 a relationship between copepod abundance with a particulate field rather than
126 chlorophyll-a. Such findings are facilitated by the fact imagery data records an
127 individual's exact position. Additionally, a copepod's true appearance, includ-
128 ing difficult to record metrics like transparency, can be measured. Thus, in-situ
129 imaging offers a new perspective to investigate DVM hypotheses. Some studies
130 observed a copepod DVM pattern with in-situ imagery data (Pan et al. 2018;
131 Whitmore and Ohman 2021). However, direct tests of DVM-related hypotheses
132 with such data have not yet been conducted.

133 In this study, we utilized in-situ imaging to evaluate how copepod morpholog-
134 ical traits influence DVM patterns. We specifically test the hypotheses that,

135 (H1) as size increases visual risk, increases in body size will increase DVM mag-
136 nitude and (H2) if copepod transparency can reduce visual risk, increases in
137 transparency will reduce DVM magnitude. If these morphologically based hy-
138 potheses are true, then the larger and darker copepods will have the largest
139 DVM magnitude.

140 **3 Methods**

141 **3.1 CTD profiles and UVP imaging of copepods**

142 Data were collected aboard the R/V Atlantic Explorer in collaboration with the
143 Bermuda Atlantic Time-series Study (BATS) (Steinberg et al. 2001). In-situ
144 images of plankton were acquired using an Underwater Vision Profiler (UVP5)
145 (Picheral et al. 2010). The original sampling methodology and instrument
146 specification followed details described in Barth and Stone (2022). The UVP was
147 attached to the CTD rosette and deployed regularly on cruises to the Sargasso
148 Sea from June 2019 - December 2021. Typical monthly cruises included ~13
149 profiles with average descents to 1200m (Supplemental Figure S1). In this study,
150 we investigated general trends in DVM by pooling together casts across multiple
151 cruises. This approach is necessitated by the small sampling volume of the UVP
152 (1.1L/image) and low abundance of plankton which requires aggregation of data
153 to resolve trends (see details in Barth and Stone 2022). While there was minor
154 variation between cruises (Supplemental Figure S2), this oligotrophic system is
155 relatively consistent across seasons (Steinberg et al. 2001). Additionally, every

156 cruise had an approximately equal number of day and night casts. Profiles
157 were assigned to be day or night based on locally calculated nautical dawn and
158 nautical dusk times using the R package **suncalc** 0.5.1.

159 The UVP records images of large particles ($>600\mu\text{m}$ equivalent spherical diam-
160 eter, ESD). However, living particles are not reliably identifiable below $900\mu\text{m}$
161 (Barth and Stone 2022). All recorded images were processed using Zooprocess
162 (Gorsky et al. 2010), which provides several metrics related to size, grey value,
163 and shape complexity. These features were then used to automatically sort im-
164 ages using Ecotaxa (Picheral et al. 2017). All images were manually verified
165 by the same trained taxonomist. In total, 294,913 images were recorded. Of
166 these, 85.2% were images of debris or artefacts. The smallest identified copepod
167 was 0.940mm ESD and the largest was 5.904mm ESD. Across all casts, cope-
168 pods were the most common organism, composing 58.7% of all identified, living
169 particles. In total, there were 4151 individual copepods images.

170 3.2 Morphological Grouping

171 Zooprocess measures and collects several morphologically relevant parameters.
172 To create relevant groups of copepods, a dimension reduction approach was used.
173 Similar methods have been successfully utilized to provide novel insights to ma-
174 rine snow (Trudnowska et al. 2021; Szeligowska et al. 2021), copepod dynamics
175 in the Arctic (Vilgrain et al. 2021), and temporal trends in phytoplankton com-
176 munities (Sonnet et al. 2022). First, 18 morphologically relevant parameters
177 were selected to be included in a Principal Components Analysis (PCA), fol-

178 lowing (Vilgrain et al. 2021). Parameters can be described as relating to size
179 (e.g. major axis, equivalent spherical diameter [ESD]), grey intensity (e.g. mean
180 grey value at 625nm wavelength light), shape (e.g. elongation, symmetry), and
181 shape complexity (e.g. fractal dimension). Grey-value intensity specifically can
182 capture a variety of characteristics related to particle transparency (Gorsky et
183 al. 2010). Note that the UVP5 utilizes a narrow band pass filter set to 625
184 nm, removing the effect of ambient lighting on particle transparency metrics
185 (Picheral et al. 2010). Feeding these multiple metrics into a morphospace analy-
186 sis has several advantages. First, Principle Components establish the major axes
187 of variability which can aid in interpreting the relative importance of different
188 traits. Furthermore, in the context of this study, there are several factors which
189 influence copepod transparency which are not easily distinguishable in most
190 UVP images. If only one metric was selected it may only capture one aspect of
191 transparency, thus by including all factors, we can create a composite metric.
192 Such approaches have been utilized successfully to infer characteristics in in-situ
193 imaged marine snow (Trudnowska et al. 2021; Szeligowska et al. 2021).
194 The PCA was weighted by the volume sampled in a 1-m depth bin for each
195 observation. This approach provides a correction for the UVP's variable descent
196 speed which can cause duplicate imaging of individuals. While this phenomena
197 has a minor impact on overall results (Barth and Stone 2022), we used the
198 weighted approach to assure that no individual features were overrepresented.
199 All morphological descriptors were scaled and centered prior to inclusion in the
200 analysis. The model was constructed using the R package **FactoMineR** 2.7.

²⁰¹ Principal Components (PCs) were deemed to be significant if their eigenvalues
²⁰² were greater than 1. This approach yielded 4 PCs which described 87.3% of
²⁰³ the total variation in morphological parameters, with 34.5% and 26.5% in the
²⁰⁴ first two components respectively. The third and fourth PCs were related to the
²⁰⁵ orientation of the copepod and appendage visibility respectively. Presumably,
²⁰⁶ this is an artifact of how the copepod was imaged. Because all axes in a PCA
²⁰⁷ are orthogonal to one another, the variation captured by PC1 and PC2 are
²⁰⁸ largely spread evenly across the copepod image variability (PC3 & PC4). This
²⁰⁹ is a particularly useful feature as copepod orientation presumably impacts some
²¹⁰ metrics such as size and grey-value. Yet, because orientation is largely accounted
²¹¹ for with PC3, by grouping along the first two PCs, variation attributable to
²¹² orientation is homogeneous across those axes.

²¹³ To address our morphology-DVM hypotheses, we constructed discrete morpho-
²¹⁴ logical groups based on the first two principal components. Groups along each
²¹⁵ of the principal components were defined as low (below 25th percentile), mid
²¹⁶ (25th-75th percentile) and high (greater than 75th percentile). To address the
²¹⁷ size-dependent hypothesis (H1), groups were assigned as low, mid, or high along
²¹⁸ PC1. Then to assess if color/transparency was a secondary factor (H2), within
²¹⁹ each PC1 group, PC2 groups were constructed as low, mid, or high. In total,
²²⁰ this created 9 groups (e.g. Low PC1-Low PC2, Low P1-mid PC2, etc).

221 **3.3 Copepod vertical structure & DVM**

222 **3.3.1 Vertical distribution of copepods**

223 Copepods in this system are well documented to undergo DVM (Steinberg et
224 al. 2000; Schnetzer and Steinberg 2002; Maas et al. 2018). However, there
225 have not been direct measurements of DVM with in-situ imaging data. First, to
226 assess which portion of the water column copepods were utilizing for DVM, we
227 visualized the average vertical structure. The concentrations of each morpholog-
228 ical group (based on PC1 and PC2) were calculated in 20m depth bins for each
229 UVP profile. Profiles were designated as either day or night. Then across all
230 day/night profiles, the mean concentration was calculated for each 20m depth
231 bin.

232 **3.3.2 Weighted mean depth variability**

233 Weighted mean depth (WMD) is a common metric to describe vertical structure
234 and DVM in zooplankton (Ohman et al. 2002; Ohman and Romagnan 2016;
235 Aarflot et al. 2019). However, with in-situ imagery and our particular dataset,
236 this approach presents a few challenges. WMD cannot be calculated individually
237 for each profile then averaged because many profiles in this study had different
238 descent depths. Additionally, the small and uneven sampling volume of the
239 UVP can make single casts too variable to reliably resolve abundance. Yet, un-
240 derstanding variation around the WMD is necessary to compare DVM strength
241 across groups. Here, we introduce a depth-bin constrained bootstrap approach
242 to define WMD with a 95% confidence interval. To do this, the concentration of

243 each group, was calculated in 20m depth bins for each profile. Then all profiles
 244 were ‘pooled’, separately for day/night. This provides a distribution of concen-
 245 trations in each depth-bin. Pooling across multiple seasons was necessary to
 246 have sufficient data, however it does introduce additionally variability. Due to
 247 the different descent speeds and depth of profiles, there are more observations
 248 of surface depth bins. Thus, traditional bootstrapping would bias estimate to-
 249 ward the surface as resampling would be more likely to draw a more-frequently
 250 observed surface bin. To avoid this, bootstrap samples were “bin-constrained”
 251 such that for each iteration, a random observation was drawn within each depth
 252 bin, then replaced for the next iteration. A maximum depth was set to 600m
 253 based on qualitative observations of vertical profiles. This approach effectively
 254 created a random profile by resampling a concentration, $conc^*$, from each depth
 255 bin, d . For each iteration, the random constructed profile then was used to cal-
 256 culate a bootstrapped weighted mean depth, WMD^* . This was done for each
 257 morphological group, g , at each time of day, t (day/night).

$$WMD_{g,t}^* = \sum_i^{N=30} \frac{d_i(conc_{i,g,t}^*)}{\sum_i^{N=30} conc_{i,g,t}^*}$$

258 The distribution of $WMD_{g,t}^*$ then was used to calculate a bootstrapped mean
 259 and 95% confidence interval. The width of the confidence interval then is influ-
 260 enced both by the spread of copepods through the water column and the amount
 261 of data available to confidently support their estimates. Thus, this resampling
 262 approach is conservative in identifying a significant trend. The conservative

263 approach is desirable given both its robustness to UVP sampling variability and
264 the need to pool casts as described above. To assess a DVM pattern, the 95%
265 CIs can be compared between times of day and morphological groups. We define
266 a clear DVM signal (e.g. significant day/night difference) as when there is no
267 overlap between the 95% WMD CIs between nighttime and daytime
268 groups. If a clear signal was observed, the DVM magnitude can be measured
269 by comparing the mean *WMD**s.

270 With PC1 to assess the size-based hypothesis (H1), the WMD was compared
271 between the three PC1-groups by percentile level. Then to assess the effect of
272 transparency (H2) the WMD was compared between PC2-groups within each
273 PC1-grouping.

274 4 Results

275 4.1 Morphological Groups

276 The PCA revealed four major axes of variability (Figure 1). The first axis (PC1,
277 34.23% of variability) was largely explained by increasing values related to size,
278 such as perimeter (loading score = 0.927) and feret diameter (maximum distance
279 between parallel planes around an object) (loading score = 0.910). The second
280 axis (PC2, 27.24% of variability) can be interpreted as a gradient of transparent
281 to dark individuals. PC2 was largely anticorrelated with mean grey value (higher
282 values indicate a more transparent individual) (loading score = -0.920). As
283 noted in the methods, PC3 and PC4 were both related to the orientation of the

²⁸⁴ copepod and the appendage visibility respectively (Supplemental Figure 3).

²⁸⁵ The morphological groupings were assigned along PC1 as low, mid and high.

²⁸⁶ Then along PC2, groups were assigned within each PC1-group (Figure 1). To

²⁸⁷ confirm the morphospace grouping resulted in ecologically relevant categories,

²⁸⁸ the morphological groups were compared against known copepod metrics.

²⁸⁹ Across all PC1-groups, there was a clear difference in feret diameter. The

²⁹⁰ median feret diameter of the low group was 1.97mm. The median feret diameter

²⁹¹ of the mid and high groups were 2.84mm and 4.83mm, respectively (Figure 2A).

²⁹² All groups were significantly different from one another (Dunn Kruskall-Wallace

²⁹³ test, $p < 0.001$). PC2 groups as a whole were also significantly different from

²⁹⁴ one another (Dunn Krustall-wallace test, $p < 0.001$). However, within each

²⁹⁵ PC2-group, there was a clear tendency for larger copepods (high PC1 group)

²⁹⁶ to be more transparent (Figure 2B).

²⁹⁷ **4.2 Vertical Profiles of Morphological Groups**

²⁹⁸ For all groups, the 20m-binned profiles show a notable structure. While cope-

²⁹⁹ pods were observed throughout the mesopelagic (Supplemental Figure 4), the

³⁰⁰ majority of day/night differences were observed above 600m (Figure 3). For

³⁰¹ most morphological groups, there was a peak in nighttime concentration in the

³⁰² lower epipelagic (50m-200m). Similarly, there was a decrease in average day-

³⁰³ time concentration over the same region. This pattern is particularly apparent

³⁰⁴ for the groups which are mid and high on both PCs (Figure 3B, C, E, F). Across

³⁰⁵ all groups, both average daytime and nighttime concentration were low in the

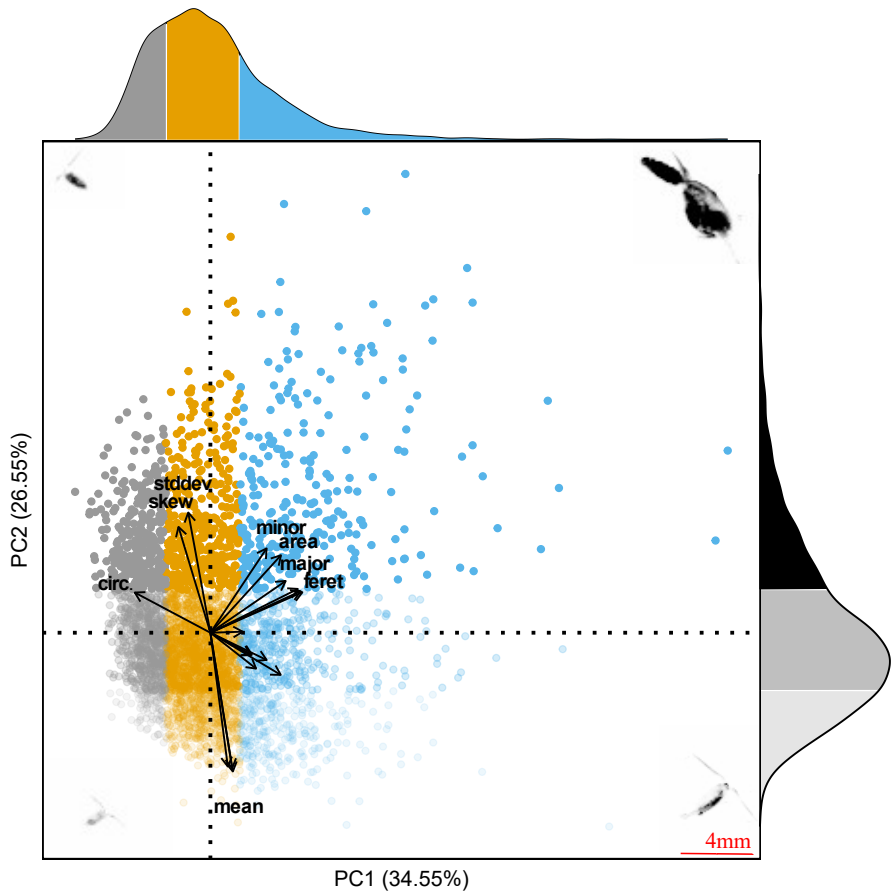


Figure 1: First two principal components of the morphospace. Proportion of variance explained by the two axis is 61.1%. Each point represents an individual copepod. The color and transparency of each point corresponds to the morphological groups based on percentile along each axis. Along PC1, grey corresponds to the low-group (<25th percentile), orange to the mid group (25th-75th percentiles), and blue to the high-group (75th percentile). Along PC2, low, mid, and high groups are distinguished by increasing opacity. Marginal distribution display the proportion of observations in each group. Representative vignettes of copepods are shown in the corners corresponding to their place in the morphospace. 4mm scale bar in the bottom right is shown for the vignettes.

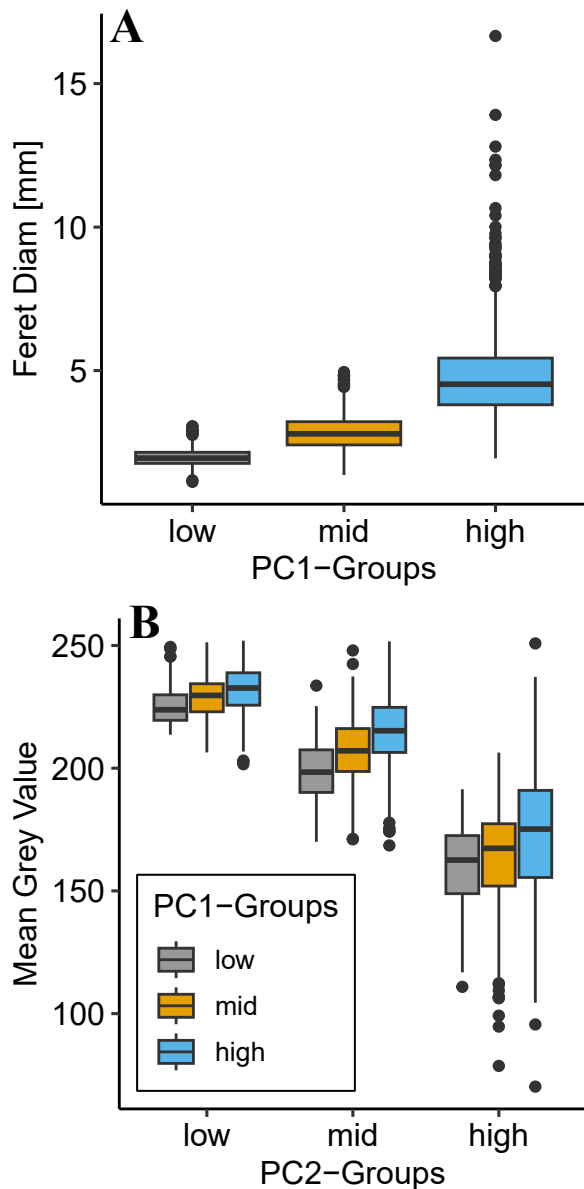


Figure 2: Comparison of morphological groups to relevant parameters. Groups were constructed along principal components with low as below 25th percentile, mid as 25th-50th percentile, and high as above 75th percentile. (A) PC1 groups are significantly different along feret diameter and display a clear trend for size. (B) PC2 groups are significantly different in terms of mean grey value. Note that a low mean grey value indicates a darker copepod.

³⁰⁶ upper mesopelagic (200m-300m). Then, there was a peak in average daytime
³⁰⁷ concentration in the depth bins in the mid-mesopelagic (400m-600m).

³⁰⁸ 4.3 Weighted mean depth analysis

³⁰⁹ The bin-constrained bootstrap approach provided a direct method to compare
³¹⁰ DVM between groups. Size (PC1) had a clear effect on DVM magnitude. First,
³¹¹ for all PC1 groups, daytime WMD 95% bootstrapped confidence intervals (95%
³¹² CIs) were deeper and non-overlapping with the nighttime 95% CIs (Figure 4).
³¹³ This indicates a clear DVM pattern. However, the differences in day and night
³¹⁴ CIs varied between morphological groups. All PC1 groups had a similar, over-
³¹⁵ lapping nighttime 95% CI in the lower epipelagic (~145m - ~200m). However,
³¹⁶ there was a clear difference in the depth of the daytime 95% CIs. The small
³¹⁷ (low PC1) group had the shallowest 95% CI (235.2m-296.0m). The mid PC1
³¹⁸ group's daytime 95% CI was slightly deeper (309.0m-347.3m). The large (high
³¹⁹ PC1) group daytime 95% CI was even lower (352.3m-405.0m).

³²⁰ When considering the influence of transparency (PC2) on DVM magnitude, we
³²¹ compared PC2 groups within their PC1 grouping. This approach was warranted
³²² because of the tendency for size to have a slight effect on transparency (Figure
³²³ 2). At this level of comparison, there were several notable trends. For the
³²⁴ smaller copepods (low PC1), once the data were split into PC2 groups, the
³²⁵ wider 95% CIs indicate little to no DVM signal. Generally, the daytime 95%
³²⁶ CIs and nighttime 95% CIs are overlapping or near-overlapping (Figure 5A).
³²⁷ With mid-sized copepods, there was a clear DVM signal. However, all PC2

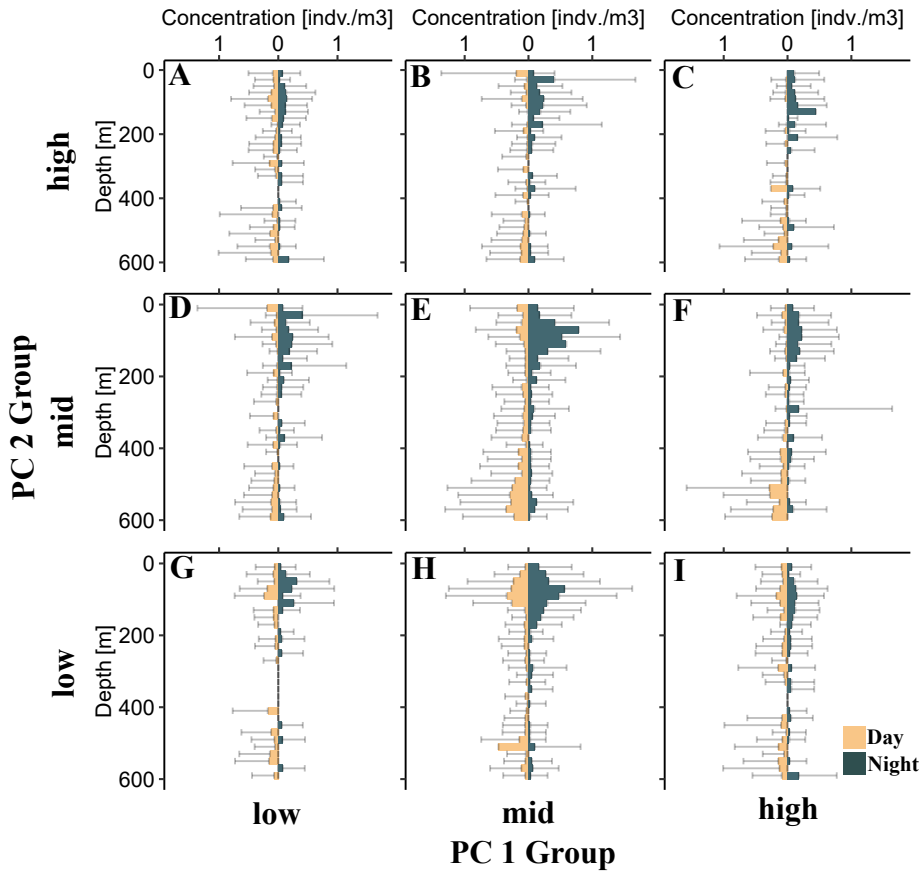


Figure 3: Average vertical profile of different copepod morphological groups. Bars display average concentration in a 20m depth bin. On each panel, left-side bars (tan) correspond to daytime while right-side (teal) bars correspond to nighttime. Standard deviation is shown for each 20m depth bin. Each panel corresponds to a morphological group along PC1 (size axis) and PC2 (transparency axis). (A) low PC1, high PC2; (B) mid PC1, high PC2; (C) high PC1, high PC2; (D) low PC1, mid PC2; (E) mid PC1, mid PC2; (F) high PC1, mid PC2; (G) low PC1, low PC2; (H) mid PC1, low PC2; (I) high PC1, low PC2

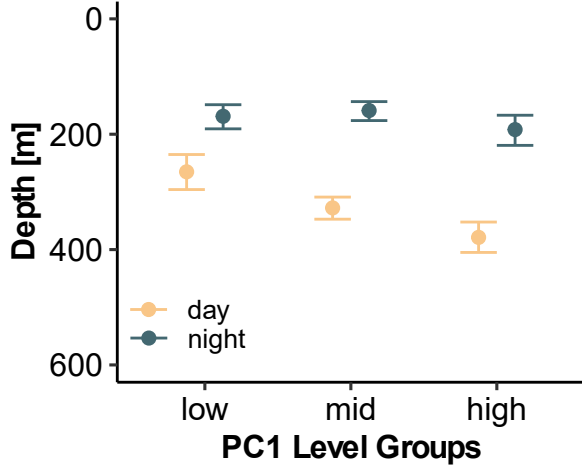


Figure 4: Mean bootstrapped weighted mean depth and 95% confidence intervals for copepods of different morphological groups. Low, mid, and high groups correspond to the different percentiles along PC1 from the morphospace. PC1 largely is explained by size metrics, with higher scores indicating a larger copepod.

328 groups appeared to have a similar DVM magnitude with each group's daytime
 329 95% CIs overlapping with each other (Figure 5B). There was a difference in
 330 DVM magnitude across PC2 groups within the largest copepods. The more
 331 transparent copepods (low PC2 group) showed no DVM signal, with a shallow
 332 daytime WMD. However, the darker copepods (mid and high PC2 groups) had
 333 deeper daytime WMDs (Figure 5c).

334 5 Discussion

335 5.1 Copepod morphospace & quantifying DVM

336 In this study, we built on methods for describing morphospaces from similar
 337 in-situ imaging studies (Vilgrain et al. 2021; Trudnowska et al. 2021; Sonnet

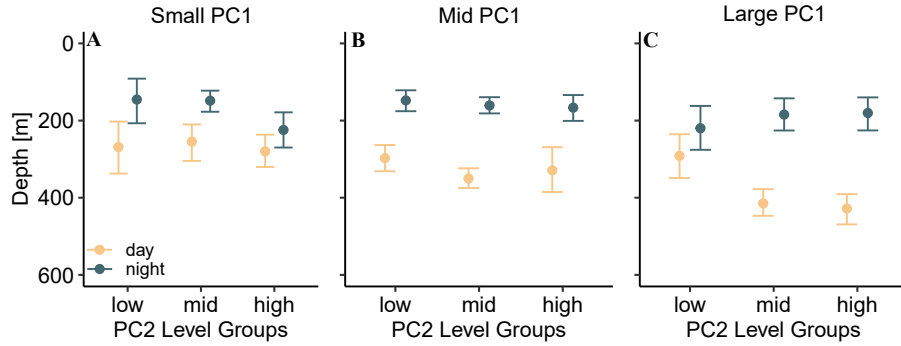


Figure 5: Mean bootstrapped weighted mean depth and 95% confidence intervals shown by copepod morphological groups along PC2 (transparency). Each panel represents a different size group of copepods (PC1 groups).

et al. 2022). The PCA-defined morphospace with the present data aligns well with the prior applications. Interestingly, the proportion of morphological variation explained by each axis in the morphospace defined on Arctic copepods by Vilgrain et al. (2021) is extremely similar to the morphospace axes in this study. This similarity is striking considering the vastly different copepod community compositions between the Arctic ocean and subtropical gyres (Soviadan et al. 2022). The similarity of morphospaces could also be an artifact of the similarity of input data. Given the UVP has a limited range of observable size classes (Picheral et al. 2010), only copepods above a certain size were fed into both PCAs. Alternatively, the similarity of studies suggest that copepod morphological variation might be well described by these two primary axes. (Sonnet et al. 2022) used phytoplankton images to investigate how a morphospace could be used to evaluate community composition changes over time. Comparisons of copepod morphospaces across temporal and spatial scales may offer a useful metric for answering biogeographic and ecological questions.

353 While the UVP provides some methodological challenges to quantifying DVM,
354 the pattern of DVM described in this study is consistent with the commonly
355 observed nocturnal DVM pattern (Bianchi and Mislan 2016; Bandara et al.
356 2021). The average vertical profiles display a clear day/night difference (Figure
357 3). However, in each 20m depth bin there was large variation, often exceeding
358 the average concentration. This large variation was expected. There can be con-
359 siderable variation between UVP estimates of zooplankton abundance (Barth
360 and Stone 2022). Additionally, in this study we pooled casts across multiple
361 seasons. Variability in copepod DVM has been described across seasons (Whit-
362 more and Ohman 2021). However, in the Sargasso Sea, while there is seasonal
363 variation in DVM biomass (Behrenfeld 2014), there is no record of variation
364 in DVM magnitude. Other studies describing DVM in the region have also
365 pooled across seasons using net data (Ivory et al. 2019). Thus, while pooling
366 across seasons may have introduced some variability in our WMD estimates,
367 the DVM signal was still well described by the UVP. Previous studies using in-
368 situ imaging have also noted a signal of DVM with copepods (Pan et al. 2018;
369 Whitmore and Ohman 2021). Yet due to small and uneven sampling, it can be
370 a challenge to quantify DVM using in-situ imaging. As presented in this paper,
371 bin-constrained bootstrapping offers a robust method to quantify WMD and
372 investigate DVM hypotheses.

³⁷³ **5.2 Morphological variation in DVM**

³⁷⁴ The results presented in this study provide new perspective on how traits influ-
³⁷⁵ ence DVM patterns. Consistent with the size-based hypothesis (H1), we docu-
³⁷⁶ mented a clear effect in which larger copepods migrated further. This finding
³⁷⁷ is consistent with several studies which have documented a size-dependent rela-
³⁷⁸ tionship for copepod DVM (Ohman and Romagnan 2016; Aarflot et al. 2019;
³⁷⁹ Pinti et al. 2019). Ohman and Romagnan (2016) noted that moderate-size
³⁸⁰ copepods had the largest migrations. While this may seem contradictory to
³⁸¹ the present study, the difference between study systems needs be taken into
³⁸² account. The copepods described in the large (high PC1) group had a mean
³⁸³ feret diameter of nearly 5mm. Conversely, in Ohman and Romagnan (2016)'s
³⁸⁴ study the "moderate" copepods ranged from 4mm-6mm.

³⁸⁵ The transparency-based hypothesis (H2) was only supported by patterns within
³⁸⁶ the large copepod group. The large but more transparent copepods (low PC2,
³⁸⁷ high PC1) did not have a detectable DVM signal. Yet the darker copepods (mid
³⁸⁸ and high PC2) had a large DVM signal. It should be noted that the grey-value
³⁸⁹ recorded by the UVP may be indicative of many features which influence cope-
³⁹⁰ pod pigmentation, including pigmentation, egg-sacs and gut contents (Vilgrain
³⁹¹ et al. 2021). Thus, while our observation is consistent with both the predator-
³⁹² avoidance and the hunger-satiation hypotheses, we cannot distinguish exactly
³⁹³ why the large, more transparent copepods do not migrate. One possibility is
³⁹⁴ that these copepods have empty gut contents, and thus are less transparent

395 and motivated to feed near the surface. However it is also plausible that the
396 difference in transparency is driven by taxonomic differences in pigmentation.
397 UVP images of copepods are generally unidentifiable to higher taxonomic reso-
398 lution. However, it is likely that the majority of copepod images were Calanoida,
399 which are consistently reported as the dominant copepod group in the Sargasso
400 Sea (Deevey and Brooks 1977; Ivory et al. 2019; Blanco-Bercial 2020). Addi-
401 tionally, a long-term analysis of net-collected data reported only Calanoida to
402 show a significant DVM signal (Ivory et al. 2019). However, within this group,
403 there is extreme diversity (Deevey and Brooks 1977; Blanco-Bercial 2020). In
404 a metabarcoding study of the epipelagic mesozooplankton community, Blanco-
405 Bercial (2020) reported *Pleuromamma spp.*, Euchaetidae, and Eucalanoidae to
406 show higher nighttime relative abundance. Alternatively, Calanidae were de-
407 scribed to occupy the surface waters at daytime. Thus, while the present study
408 cannot make direct conclusions as to taxonomic variation, it is likely a driving
409 factor in DVM variability across the observed morphological groups.
410 Hays (2003) described that copepod pigmentation could explain increased DVM
411 with small (<1mm) copepods. Thus it was surprising that there was no effect
412 of transparency on DVM magnitude in the smaller morphology group. One
413 possibility is that the small, transparent copepods were not well sampled by the
414 UVP (Figure 2). Due to the conservative nature of the bootstrapping WMD
415 approach utilized in this study, sampling deficits would broaden the 95% WMD
416 CI's, reducing the ability to resolve trends. However, there is no observable
417 trend to suggest the lack of DVM signal is simply a methodological artifact.

418 Alternatively, there are several possible explanations for why there is no effect
419 of transparency for the smaller copepod morphological groups. First, it should
420 be noted that while both the small-sized (low PC1) and mid-sized (mid-PC1)
421 group showed no variation in DVM patterns across PC2, the mid-sized group
422 consistently showed a strong DVM signal while the small-sized group did not.
423 Amongst the small-sized group, there was little observable DVM across all trans-
424 parency groupings. It may be that these copepods have a low visual-predator
425 risk regardless of their transparency level. Ohman and Romagnan (2016)'s study
426 in the California Current observed that the smallest copepods (<1.5mm) dis-
427 played no DVM signal. While these copepods may have reduced predator risk,
428 it may also be that they simply are weaker swimmers and cannot reasonably
429 migrate as large of distances as bigger copepods can.

430 The mid-sized copepods display a clear DVM signal across all transparency
431 groupings. This suggests that mid-sized copepods do not relieve their predation
432 risk through increased transparency. This is counterintuitive to the observation
433 that the large, transparent copepods have a reduced DVM signal. Additionally
434 the transparent, mid-sized copepods migrating while the transparent, large ones
435 do not, directly contradicts the predator-avoidance hypothesis. It is worth not-
436 ing that DVM behavior can also vary greatly across species. Within migrating
437 nekton, there has been mixed support described for the hunger-satiation hy-
438 pothesis, depending on taxa (Bos et al. 2021). Thus again it may be taxonomic
439 variation which can explain deviations in expected DVM patterns. Additionally,
440 other mechanisms influencing DVM, aside from top-down factors may be at

play. Williamson et al. (2011) provides support for the transparency-regulator hypothesis of DVM, which suggests both top-down factors and environmental factors such as UV-radiation influence DVM behavior. In the Sargasso Sea, there is extreme water clarity which would suggest UV-radiation may play a role in DVM behavior. However, none of our findings suggest that more pigmented copepods migrate less than transparent ones, regardless of size. Yet, across all copepod morphological groups, abundances were highest in the mid-to-lower mesopelagic and low in the surface layers (Figure 2). Thus the copepods imaged in this study are likely already at layers below where UV damage is a major factor. Furthermore, the deep chlorophyll-a maximum regularly extended into low epipelagic (Supplemental Figure S2), providing sufficient food where UV irradiance is low. Nonetheless, while UV may not be a primary factor, the notion that there are multiple factors influencing DVM should be considered.

5.3 Conclusion

Overall, our results reveal a complex dynamic between copepod traits and DVM behavior. This study provided new insight into the DVM dynamics in oligotrophic gyres. While many studies have established size as a major trait influencing DVM, investigations into other traits are more limited. Here, we support the prevailing notion that size has large consequences for DVM behavior. We also show that transparency has an effect on DVM for some size groups. However, determining exactly which drivers determine why copepods with different traits undergo diel vertical migration remains elusive. While these findings

463 are largely consistent with the predator-avoidance hypothesis and prevailing
464 DVM theory, they highlight the need for more detailed analyses. As plank-
465 ton in-situ imaging tools are used more commonly by oceanographers, larger
466 datasets will facilitate new investigations. Additionally, improved resolution
467 of sampling tools may better determine taxonomic variation. Collaborations
468 between oceanographers, plankton ecologists, and visual ecologists may better
469 resolve how traits influence trade-offs in DVM behavior. Understanding these
470 dynamics will be critical to predicting changes with a changing ocean.

471 **6 Acknowledgements**

472 Field work for this project was supported by the Bermuda Atlantic Time Series
473 Study through NSF OCE 1756105 & NSF OCE 1756312. We would also like
474 to thank the BATS research technicians, marine technicians, and crew of the
475 R/V Atlantic Explorer. Dr. Ryan Rykaczewski assisted with the initial set-up
476 of the UVP. Dr. Leo Blanco-Bercial and Dr. Amy Maas both valuable insight
477 and guidance on the analysis.

478 **6.1 References**

479 Aarflot, J. M., D. L. Aksnes, A. F. Opdal, H. R. Skjoldal, and Ø. Fiksen.
480 2019. Caught in broad daylight: Topographic constraints of zooplank-
481 ton depth distributions. Limnology and Oceanography **64**: 849–859.
482 doi:[10.1002/lno.11079](https://doi.org/10.1002/lno.11079)

483 Aksnes, D. L., and A. C. W. Utne. 1997. A revised model of visual range in

- 484 fish. *Sarsia* **82**: 137–147. doi:[10.1080/00364827.1997.10413647](https://doi.org/10.1080/00364827.1997.10413647)
- 485 Archibald, K. M., D. A. Siegel, and S. C. Doney. 2019. Modeling the
486 Impact of Zooplankton Diel Vertical Migration on the Carbon Export
487 Flux of the Biological Pump. *Global Biogeochemical Cycles* **33**: 181–199.
488 doi:[10.1029/2018GB005983](https://doi.org/10.1029/2018GB005983)
- 489 Atkinson, A., P. Ward, R. Williams, and S. A. Poulet. 1992. Diel vertical
490 migration and feeding of copepods at an oceanic site near South Georgia.
491 *Marine Biology* **113**: 583–593. doi:[10.1007/BF00349702](https://doi.org/10.1007/BF00349702)
- 492 Bandara, K., Ø. Varpe, R. Ji, and K. Eiane. 2019. Artificial evolution of
493 behavioral and life history strategies of high-latitude copepods in response
494 to bottom-up and top-down selection pressures. *Progress in Oceanography*
495 **173**: 134–164. doi:[10.1016/j.pocean.2019.02.006](https://doi.org/10.1016/j.pocean.2019.02.006)
- 496 Bandara, K., Ø. Varpe, L. Wijewardene, V. Tverberg, and K. Eiane. 2021.
497 Two hundred years of zooplankton vertical migration research. *Biological
498 Reviews* **96**: 1547–1589. doi:[10.1111/brv.12715](https://doi.org/10.1111/brv.12715)
- 499 Barth, A., and J. Stone. 2022. **Comparison of an in situ imaging device and
500 net-based method to study mesozooplankton communities in an oligotrophic
501 system.** *Frontiers in Marine Science* **9**.
- 502 Behrenfeld, M. J. 2014. Climate-mediated dance of the plankton. *Nature Climate
503 Change* **4**: 880–887. doi:[10.1038/nclimate2349](https://doi.org/10.1038/nclimate2349)
- 504 Behrenfeld, M. J., P. Gaube, A. Della Penna, and others. 2019. Global satellite-
505 observed daily vertical migrations of ocean animals. *Nature* **576**: 257–261.
506 doi:[10.1038/s41586-019-1796-9](https://doi.org/10.1038/s41586-019-1796-9)

- 507 Bianchi, D., and K. a. S. Mislan. 2016. Global patterns of diel vertical migration
- 508 times and velocities from acoustic data. Limnology and Oceanography **61**:
- 509 353–364. doi:[10.1002/lno.10219](https://doi.org/10.1002/lno.10219)
- 510 Blanco-Bercial, L. 2020. Metabarcoding analyses and seasonality of the zoo-
- 511 plankton community at BATS. Frontiers in Marine Science **7**.
- 512 Bos, R. P., T. T. Sutton, and T. M. Frank. 2021. State of satiation partially
- 513 regulates the dynamics of vertical migration. Frontiers in Marine Science **8**.
- 514 Brierley, A. S. 2014. Diel vertical migration. Current Biology **24**: R1074–R1076.
- 515 doi:[10.1016/j.cub.2014.08.054](https://doi.org/10.1016/j.cub.2014.08.054)
- 516 Cohen, J. H., and R. B. Forward Jr. 2009. Zooplankton diel vertical migration:
- 517 a review of proximate control, p. 77–110. In.
- 518 Deevey, G. B., and A. L. Brooks. 1977. Copepods of the sargasso sea off
- 519 bermuda: Species composition, and vertical and seasonal distribution be-
- 520 tween the surface and 2000 m. Bulletin of Marine Science **27**: 256–291.
- 521 Enright, J. T. 1977. Diurnal vertical migration: Adaptive significance and tim-
- 522 ing. Part 1. Selective advantage: A metabolic model. Limnology and
- 523 Oceanography **22**: 856–872. doi:[10.4319/lo.1977.22.5.0856](https://doi.org/10.4319/lo.1977.22.5.0856)
- 524 Ewald, W. F. 1912. On artificial modification of light reactions and the influence
- 525 of electrolytes on phototaxis. Journal of Experimental Zoology **13**: 591–612.
- 526 doi:[10.1002/jez.1400130405](https://doi.org/10.1002/jez.1400130405)
- 527 Gorsky, G., M. D. Ohman, M. Picheral, and others. 2010. Digital zooplankton
- 528 image analysis using the ZooScan integrated system. Journal of Plankton
- 529 Research **32**: 285–303. doi:[10.1093/plankt/fbp124](https://doi.org/10.1093/plankt/fbp124)

- 530 Hays, G. C. 2003. A review of the adaptive significance and ecosystem conse-
531 quences of zooplankton diel vertical migrations. Springer Netherlands. 163–
532 170.
- 533 Hays, G. C., C. A. Proctor, A. W. G. John, and A. J. Warner. 1994. Inter-
534 specific differences in the diel vertical migration of marine copepods: The
535 implications of size, color, and morphology. Limnology and Oceanography
536 **39**: 1621–1629. doi:[10.4319/lo.1994.39.7.1621](https://doi.org/10.4319/lo.1994.39.7.1621)
- 537 Ivory, J. A., D. K. Steinberg, and R. J. Latour. 2019. Diel, seasonal, and inter-
538 annual patterns in mesozooplankton abundance in the sargasso sea. ICES
539 Journal of Marine Science **76**: 217–231. doi:[10.1093/icesjms/fsy117](https://doi.org/10.1093/icesjms/fsy117)
- 540 Kelly, T. B., P. C. Davison, R. Goericke, M. R. Landry, M. D. Ohman, and M.
541 R. Stukel. 2019. The importance of mesozooplankton diel vertical migration
542 for sustaining a mesopelagic food web. Frontiers in Marine Science **6**.
- 543 Kessler, K., R. S. Lockwood, C. E. Williamson, and J. E. Saros. 2008. Vertical
544 distribution of zooplankton in subalpine and alpine lakes: Ultraviolet radi-
545 ation, fish predation, and the transparency-gradient hypothesis. Limnology
546 and Oceanography **53**: 2374–2382. doi:[10.4319/lo.2008.53.6.2374](https://doi.org/10.4319/lo.2008.53.6.2374)
- 547 Lampert, W. 1989. The adaptive significance of diel vertical migration of zoo-
548 plankton. Functional Ecology **3**: 21–27. doi:[10.2307/2389671](https://doi.org/10.2307/2389671)
- 549 Liu, Y., J. Guo, Y. Xue, C. Sangmanee, H. Wang, C. Zhao, S. Khokiattiwong,
550 and W. Yu. 2022. Seasonal variation in diel vertical migration of zooplank-
551 ton and micronekton in the andaman sea observed by a moored ADCP.
552 Deep Sea Research Part I: Oceanographic Research Papers **179**: 103663.

- 553 doi:[10.1016/j.dsr.2021.103663](https://doi.org/10.1016/j.dsr.2021.103663)
- 554 Maas, A. E., L. Blanco-Bercial, A. Lo, A. M. Tarrant, and E. Timmins-
- 555 Schiffman. 2018. Variations in copepod proteome and respiration rate in
- 556 association with diel vertical migration and circadian cycle. *The Biological*
- 557 *Bulletin* **235**: 30–42. doi:[10.1086/699219](https://doi.org/10.1086/699219)
- 558 McLaren, I. A. 1963. Effects of temperature on growth of zooplankton, and
- 559 the adaptive value of vertical migration. *Journal of the Fisheries Research*
- 560 *Board of Canada* **20**: 685–727. doi:[10.1139/f63-046](https://doi.org/10.1139/f63-046)
- 561 McLaren, I. A. 1974. *Demographic strategy of vertical migration by a marine*
- 562 *copepod*. *The American Naturalist* **108**: 91–102.
- 563 Ohman, M. D. 1990. The Demographic Benefits of Diel Vertical Migration by
- 564 Zooplankton. *Ecological Monographs* **60**: 257–281. doi:[10.2307/1943058](https://doi.org/10.2307/1943058)
- 565 Ohman, M. D. 2019. A sea of tentacles: optically discernible traits resolved from
- 566 planktonic organisms *in situ* H. Browman [ed.]. *ICES Journal of Marine*
- 567 *Science* **76**: 1959–1972. doi:[10.1093/icesjms/fsz184](https://doi.org/10.1093/icesjms/fsz184)
- 568 Ohman, M. D., and J.-B. Romagnan. 2016. Nonlinear effects of body size and
- 569 optical attenuation on Diel Vertical Migration by zooplankton. *Limnology*
- 570 and *Oceanography* **61**: 765–770. doi:[10.1002/lno.10251](https://doi.org/10.1002/lno.10251)
- 571 Ohman, M. D., J. A. Runge, E. G. Durbin, D. B. Field, and B. Niehoff.
- 572 2002. On birth and death in the sea. *Hydrobiologia* **480**: 55–68.
- 573 doi:[10.1023/A:1021228900786](https://doi.org/10.1023/A:1021228900786)
- 574 Pan, J., F. Cheng, and F. Yu. 2018. The diel vertical migration of zooplankton
- 575 in the hypoxia area observed by video plankton recorder. *IJMS* Vol.47(07)

576 [July 2018].

577 Pearre, S. 2003. Eat and run? The hunger/satiation hypothesis in vertical
578 migration: history, evidence and consequences. *Biological Reviews* **78**: 1–
579 79. doi:[10.1017/S146479310200595X](https://doi.org/10.1017/S146479310200595X)

580 Picheral, M., S. Colin, and J.-O. Irisson. 2017. [EcoTaxa, a tool for the taxonomic classification of images](#).

582 Picheral, M., L. Guidi, L. Stemmann, D. M. Karl, G. Iddaoud, and G. Gorsky.
583 2010. The Underwater Vision Profiler 5: An advanced instrument for high
584 spatial resolution studies of particle size spectra and zooplankton. *Limnology*
585 and *Oceanography: Methods* **8**: 462–473. doi:[10.4319/lom.2010.8.462](https://doi.org/10.4319/lom.2010.8.462)

586 Pinti, J., T. Kiørboe, U. H. Thygesen, and A. W. Visser. 2019. Trophic interactions drive the emergence of diel vertical migration patterns: A game-theoretic model of copepod communities. *Proceedings of the Royal Society B: Biological Sciences* **286**: 20191645. doi:[10.1098/rspb.2019.1645](https://doi.org/10.1098/rspb.2019.1645)

590 Ringelberg, J. 2009. *Diel Vertical Migration of Zooplankton in Lakes and Oceans: causal explanations and adaptive significances*, Springer Science
591 & Business Media.

593 Robison, B. H., R. E. Sherlock, K. R. Reisenbichler, and P. R. McGill. 2020.
594 [Running the gauntlet: Assessing the threats to vertical migrators](#). *Frontiers in Marine Science* **7**.

596 Schnetzer, A., and D. K. Steinberg. 2002. Active transport of particulate organic carbon and nitrogen by vertically migrating zooplankton
597 in the Sargasso Sea. *Marine Ecology Progress Series* **234**: 71–84.

- 599 doi:[10.3354/meps234071](https://doi.org/10.3354/meps234071)
- 600 Siegel, D. A., T. DeVries, I. Cetinić, and K. M. Bisson. 2023. Quantifying
601 the ocean's biological pump and its carbon cycle impacts on global scales.
602 Annual Review of Marine Science **15**: null. doi:[10.1146/annurev-marine-040722-115226](https://doi.org/10.1146/annurev-marine-040722-115226)
- 603
- 604 Sonnet, V., L. Guidi, C. B. Mouw, G. Puggioni, and S.-D. Ayata. 2022. Length,
605 width, shape regularity, and chain structure: time series analysis of phy-
606toplankton morphology from imagery. Limnology and Oceanography **67**:
607 1850–1864. doi:[10.1002/lno.12171](https://doi.org/10.1002/lno.12171)
- 608 Soviadan, Y. D., F. Benedetti, M. C. Brandão, and others. 2022.
609 Patterns of mesozooplankton community composition and vertical
610 fluxes in the global ocean. Progress in Oceanography **200**: 102717.
611 doi:[10.1016/j.pocean.2021.102717](https://doi.org/10.1016/j.pocean.2021.102717)
- 612 Steinberg, D. K., C. A. Carlson, N. R. Bates, S. A. Goldthwait, L. P. Madin,
613 and A. F. Michaels. 2000. Zooplankton vertical migration and the active
614 transport of dissolved organic and inorganic carbon in the Sargasso Sea.
615 Deep Sea Research Part I: Oceanographic Research Papers **47**: 137–158.
616 doi:[10.1016/S0967-0637\(99\)00052-7](https://doi.org/10.1016/S0967-0637(99)00052-7)
- 617 Steinberg, D. K., C. A. Carlson, N. R. Bates, R. J. Johnson, A. F. Michaels,
618 and A. H. Knap. 2001. Overview of the US JGOFS Bermuda Atlantic
619 Time-series Study (BATS): a decade-scale look at ocean biology and biogeo-
620 chemistry. Deep Sea Research Part II: Topical Studies in Oceanography **48**:
621 1405–1447. doi:[10.1016/S0967-0645\(00\)00148-X](https://doi.org/10.1016/S0967-0645(00)00148-X)

- 622 Steinberg, D. K., and M. R. Landry. 2017. Zooplankton and the ocean carbon
623 cycle. *Annual Review of Marine Science* **9**: 413–444. doi:[10.1146/annurev-marine-010814-015924](https://doi.org/10.1146/annurev-marine-010814-015924)
- 624
- 625 Szeligowska, M., E. Trudnowska, R. Boehnke, A. M. Dąbrowska, K. Dragańska-
626 Deja, K. Deja, M. Darecki, and K. Błachowiak-Samołyk. 2021. The inter-
627 play between plankton and particles in the Isfjorden waters influenced by
628 marine- and land-terminating glaciers. *Science of The Total Environment*
629 **780**: 146491. doi:[10.1016/j.scitotenv.2021.146491](https://doi.org/10.1016/j.scitotenv.2021.146491)
- 630 Trudnowska, E., L. Lacour, M. Ardyna, A. Rogge, J. O. Irisson, A. M. Waite, M.
631 Babin, and L. Stemmann. 2021. Marine snow morphology illuminates the
632 evolution of phytoplankton blooms and determines their subsequent vertical
633 export. *Nature Communications* **12**: 2816. doi:[10.1038/s41467-021-22994-4](https://doi.org/10.1038/s41467-021-22994-4)
- 634 Turner, J. 2004. The importance of small planktonic copepods and their roles
635 in pelagic marine food webs,.
- 636 Vilgrain, L., F. Maps, M. Picheral, M. Babin, C. Aubry, J.-O. Irisson, and S.-D.
637 Ayata. 2021. Trait-based approach using in situ copepod images reveals
638 contrasting ecological patterns across an Arctic ice melt zone. *Limnology
639 and Oceanography* **66**: 1155–1167. doi:[10.1002/lno.11672](https://doi.org/10.1002/lno.11672)
- 640 Whitmore, B. M., and M. D. Ohman. 2021. Zooglider-measured association of
641 zooplankton with the fine-scale vertical prey field. *Limnology and Oceanog-
642 raphy* **66**: 3811–3827. doi:[10.1002/lno.11920](https://doi.org/10.1002/lno.11920)
- 643 Williamson, C. E., J. M. Fischer, S. M. Bollens, E. P. Overholt, and J. K. Breck-
644 enridge. 2011. Toward a more comprehensive theory of zooplankton diel

645 vertical migration: Integrating ultraviolet radiation and water transparency
646 into the biotic paradigm. Limnology and Oceanography **56**: 1603–1623.
647 doi:[10.4319/lo.2011.56.5.1603](https://doi.org/10.4319/lo.2011.56.5.1603)

648 Zaret, T. M., and J. S. Suffern. 1976. Vertical migration in zooplankton as a
649 predator avoidance mechanism1. Limnology and Oceanography **21**: 804–813.
650 doi:[10.4319/lo.1976.21.6.0804](https://doi.org/10.4319/lo.1976.21.6.0804)

651 **7 Data availability statement**

652 All data used in this project are hosted on Ecopart ([https://ecopart.obs-vlfr.](https://ecopart.obs-vlfr.fr/)
653 [fr/](https://ecopart.obs-vlfr.fr/)). Data in its raw form can be accessed from their portal. However, all
654 summary and intermediate data products, as well as code, are publicly available
655 on GitHub (https://github.com/TheAlexBarth/DVM_Migration-Morphology).
656 Intermediate data products are formatted as R Data Structure objects, other
657 formats are available on request.

658 **8 Supplemental Information**

	Dim.1	Dim.2	Dim.3	Dim.4
area	0.7115131	0.5137738	-0.1301928	0.3789753
circ.	-0.7627265	0.2665557	-0.3026239	0.3034329
elongation	0.4080632	-0.1487560	-0.7831847	-0.2965671
feret	0.9096148	0.2756948	-0.2479648	0.0082808

	Dim.1	Dim.2	Dim.3	Dim.4
fractal	0.8816770	0.2904962	-0.0440580	0.1793785
histcum1	0.2197180	-0.8987922	-0.0901744	0.3005361
major	0.7593652	0.3432489	-0.5115438	0.1498407
mean	0.2266145	-0.9201880	-0.0611832	0.2875560
median	0.1758116	-0.8872673	0.0657406	0.1668198
minor	0.5668215	0.5593596	0.2891461	0.4585166
perim.	0.9268957	0.2685898	0.0681774	0.1135716
perimferet	0.3251295	0.0068372	0.7989292	0.2111105
perimmajor	0.4183142	-0.1460583	0.8627707	-0.1389696
skew	-0.3216781	0.7017490	0.1514517	-0.1447764
stddev	-0.2234641	0.7971849	0.1531288	-0.3647663
symetriev	0.7091737	-0.2793593	-0.0605051	-0.5720602
symtrievc	0.5673730	-0.1807542	-0.2368157	-0.4811256
thickr	0.4609473	-0.2379533	0.5832035	-0.3954358

⁶⁵⁹ Supplemental Table S2. Loading scores for morphological factors on the PCA.

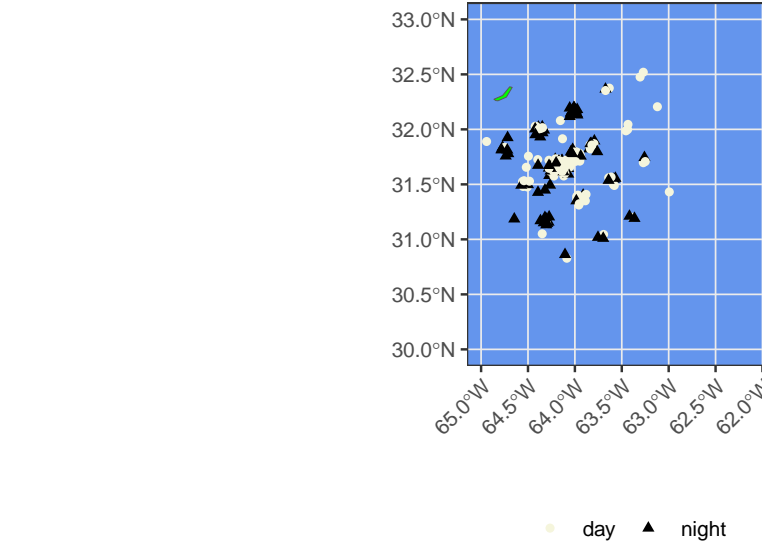


Figure 6: Supplemental Figure S1. Map of CTD Cast Deployments. Dark triangle points indicate night casts, tan circles indicate day casts.

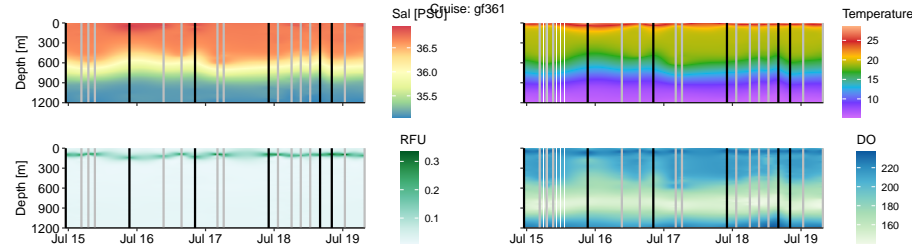


Figure 7: Supplemental Figure S2. Physical parameters across individual cruises. Vertical bars indicate CTD casts events with black indicating night and grey indicating day.

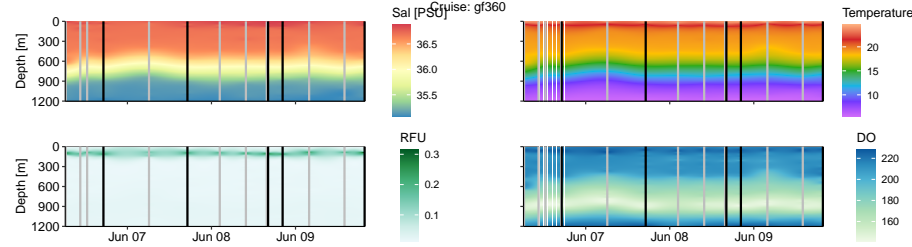


Figure 8: Supplemental Figure S2. Physical parameters across individual cruises. Vertical bars indicate CTD casts events with black indicating night and grey indicating day.

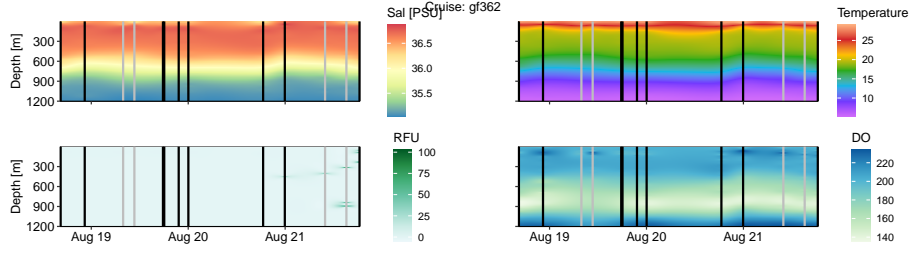


Figure 9: Supplemental Figure S2. Physical parameters across individual cruises. Vertical bars indicate CTD casts events with black indicating night and grey indicating day.

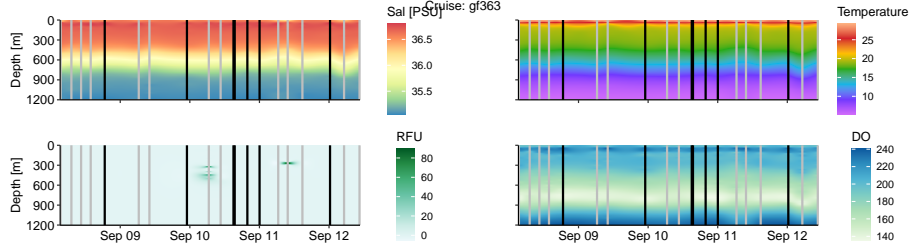


Figure 10: Supplemental Figure S2. Physical parameters across individual cruises. Vertical bars indicate CTD casts events with black indicating night and grey indicating day.

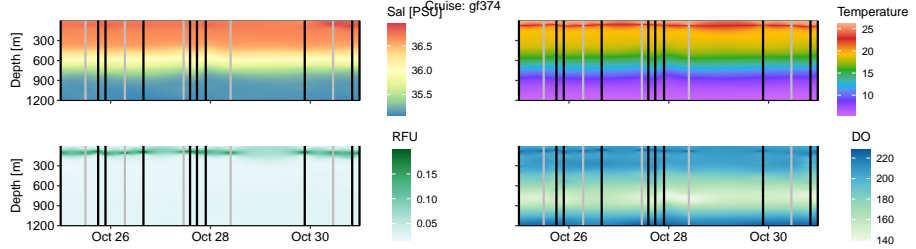


Figure 11: Supplemental Figure S2. Physical parameters across individual cruises. Vertical bars indicate CTD casts events with black indicating night and grey indicating day.

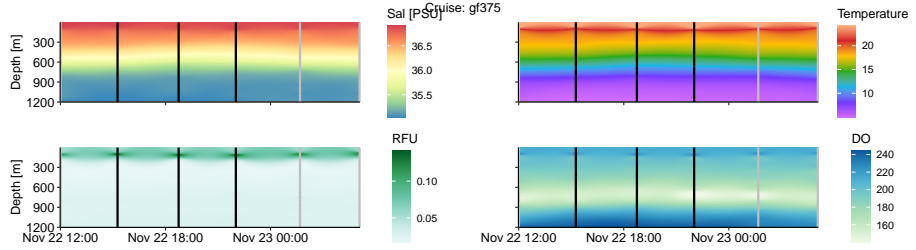


Figure 12: Supplemental Figure S2. Physical parameters across individual cruises. Vertical bars indicate CTD casts events with black indicating night and grey indicating day.

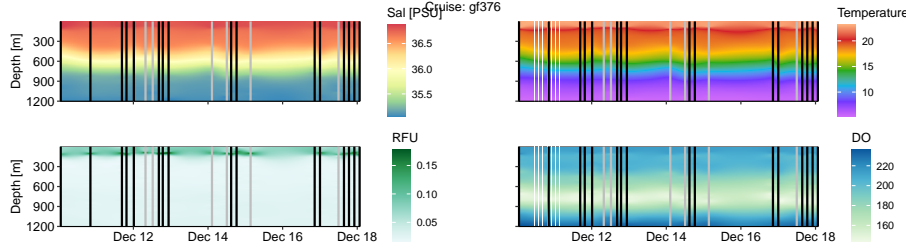


Figure 13: Supplemental Figure S2. Physical parameters across individual cruises. Vertical bars indicate CTD casts events with black indicating night and grey indicating day.

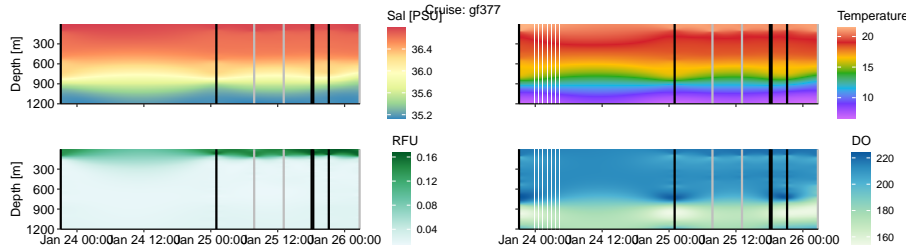


Figure 14: Supplemental Figure S2. Physical parameters across individual cruises. Vertical bars indicate CTD casts events with black indicating night and grey indicating day.

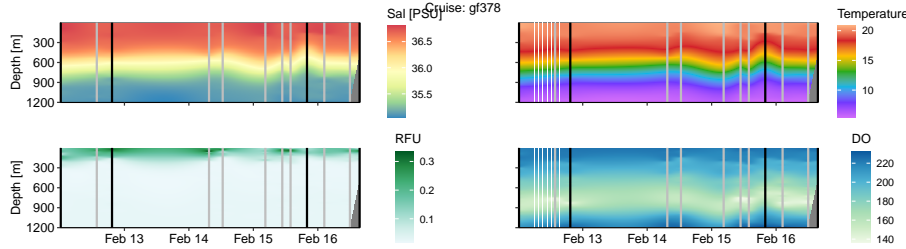


Figure 15: Supplemental Figure S2. Physical parameters across individual cruises. Vertical bars indicate CTD casts events with black indicating night and grey indicating day.

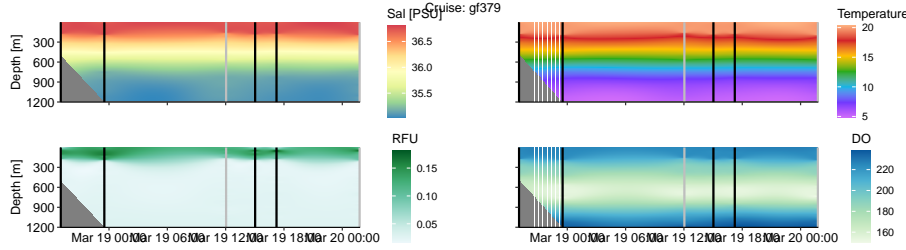


Figure 16: Supplemental Figure S2. Physical parameters across individual cruises. Vertical bars indicate CTD casts events with black indicating night and grey indicating day.

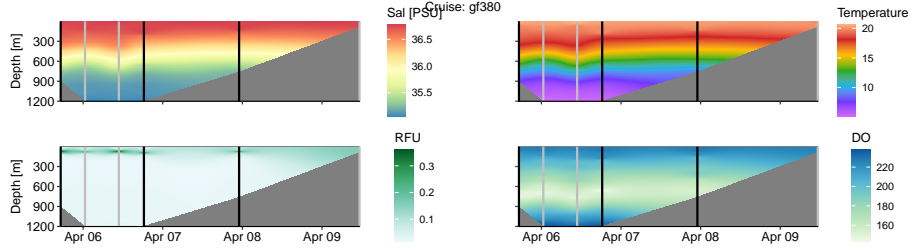


Figure 17: Supplemental Figure S2. Physical parameters across individual cruises. Vertical bars indicate CTD casts events with black indicating night and grey indicating day.

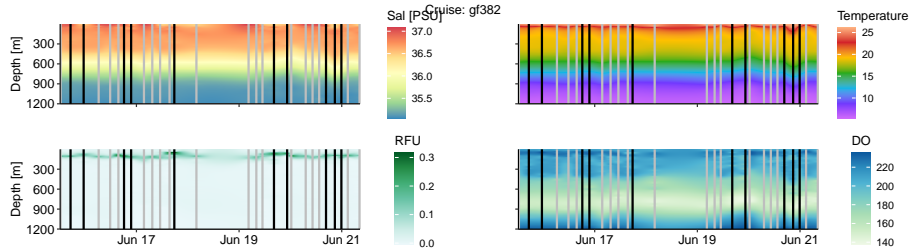


Figure 18: Supplemental Figure S2. Physical parameters across individual cruises. Vertical bars indicate CTD casts events with black indicating night and grey indicating day.

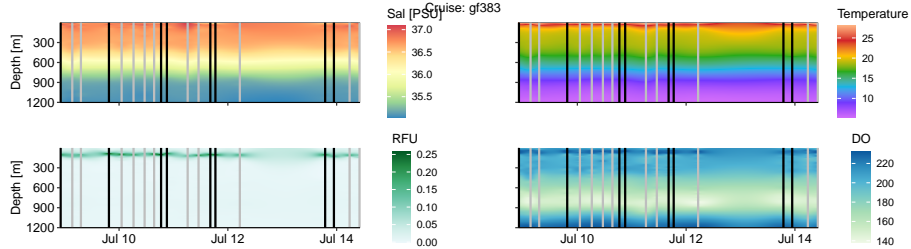


Figure 19: Supplemental Figure S2. Physical parameters across individual cruises. Vertical bars indicate CTD casts events with black indicating night and grey indicating day.

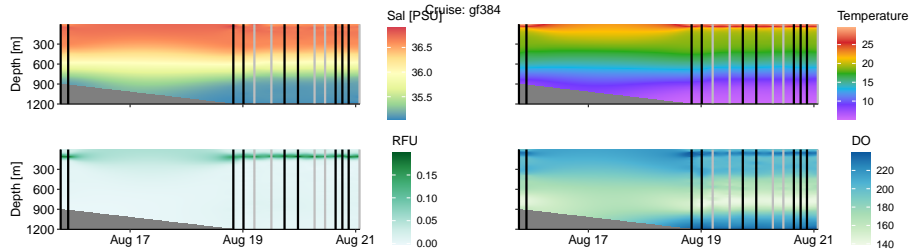


Figure 20: Supplemental Figure S2. Physical parameters across individual cruises. Vertical bars indicate CTD casts events with black indicating night and grey indicating day.

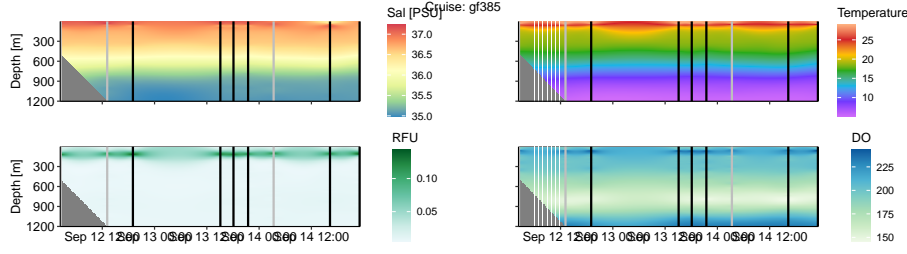


Figure 21: Supplemental Figure S2. Physical parameters across individual cruises. Vertical bars indicate CTD casts events with black indicating night and grey indicating day.

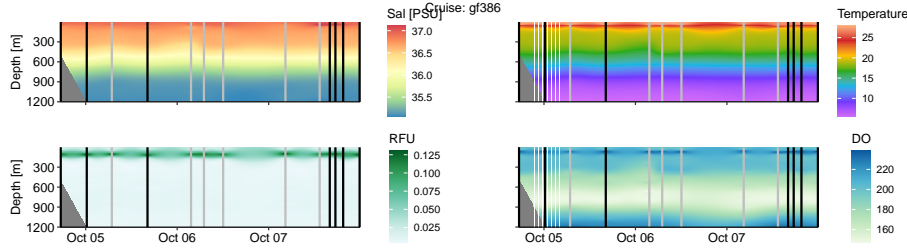


Figure 22: Supplemental Figure S2. Physical parameters across individual cruises. Vertical bars indicate CTD casts events with black indicating night and grey indicating day.

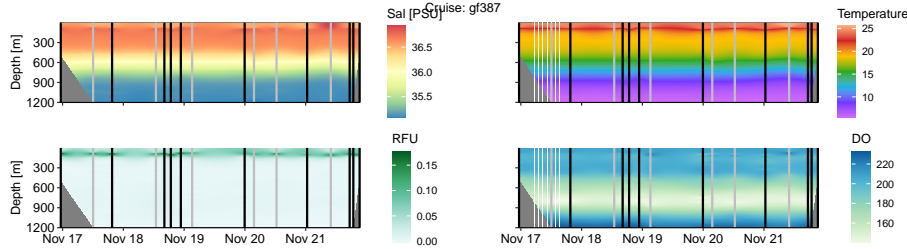


Figure 23: Supplemental Figure S2. Physical parameters across individual cruises. Vertical bars indicate CTD casts events with black indicating night and grey indicating day.

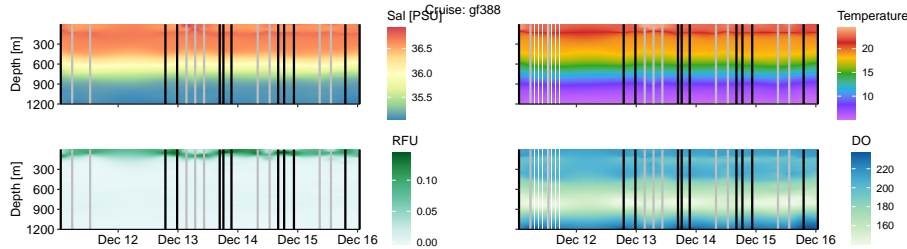


Figure 24: Supplemental Figure S2. Physical parameters across individual cruises. Vertical bars indicate CTD casts events with black indicating night and grey indicating day.

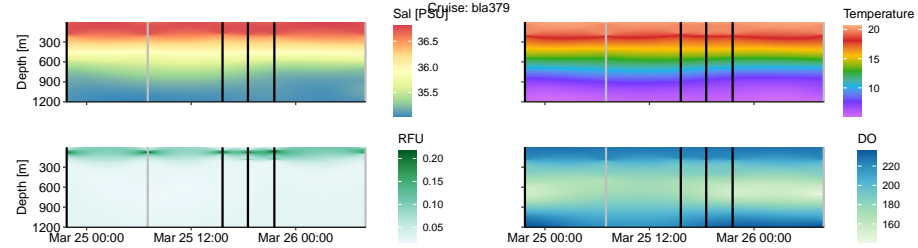


Figure 25: Supplemental Figure S2. Physical parameters across individual cruises. Vertical bars indicate CTD casts events with black indicating night and grey indicating day.

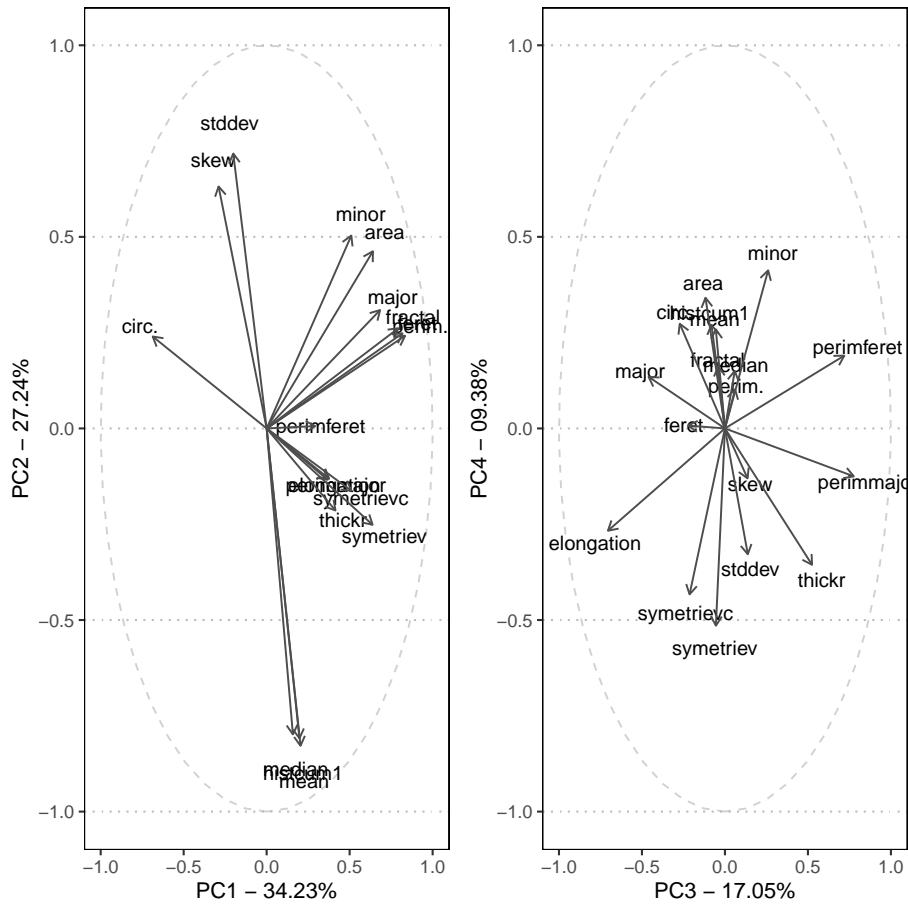


Figure 26: Supplemental Figure S3. PCA plot with major loading variables plotted.